Experimental characterization and analysis of water transport in automotive PEMFC stacks

1st Martin SERINE
Université Marie et Louis Pasteur, UTBM, CNRS, institut FEMTO-ST, FCLAB
SYMBIO
Belfort / St-Fons, France
martin.serine@symbio.one

2nd Julie AUBRY
SYMBIO
St-Fons, France
julie.aubry@symbio.one

3rd Zhixue ZHENG
Université Marie et Louis Pasteur, UTBM, CNRS, institut FEMTO-ST, FCLAB
Belfort, France
zhixue.zheng@umlp.fr

4th Daniel HISSEL
Université Marie et Louis Pasteur, UTBM, CNRS, institut FEMTO-ST, FCLAB
Institut Universitaire de France (IUF), Paris, France
Belfort, France
daniel.hissel@umlp.fr

***Abstract*—The presented work provides an experimental characterization of steady-state water transport-related metrics in automotive Proton Exchange Membrane Fuel Cell (PEMFC) stacks. Cell-level molar balance equations are formulated into a lumped model and complemented by coupling a set of differential equations describing water transport through the membrane. A back-diffusion rate is defined at both the membrane and stack scales, involving various parameters. In addition, a dedicated experimental test plan has been designed, and outlet water mass data has been collected by adding scales for liquid water to the test setup on both the anode and cathode sides. Main contributors to the water transport through the cell are identified by performing an Analysis Of Variance (ANOVA) study among controllable operating conditions. The obtained results are physically coherent with experimental data analysis and literature equations. In particular, the study confirms that water transport through PEMFC exhibits Fickian-like diffusion phenomenon primarily driven by the water concentration gradient between anode and cathode and by temperature. Furthermore, the cathode flow rate and overpressure are shown to enhance water transport. The presented work paves the way for data-driven steady-state water transport model calibration and model coupling between cell molar balance and membrane water uptake.**

***Index Terms*—Analysis Of Variance (ANOVA), experimental characterization, PEMFC stacks, water content estimation, water transport.**

I. Introduction

In a context of greenhouse gas emission reduction in the transportation sector, the demand for sustainable mobility alternative solutions is growing worldwide. Battery-powered electric vehicles (EVs) cannot address all customer needs, especially for heavy-duty transportation. Proton-Exchange Membrane Fuel Cell (PEMFC) systems offer a high-power density and reduced refueling time to address this market [1]. Since their first appearance in industrial applications, PEMFCs embrace technological breakthroughs in materials design, industrial processes, and control strategies [2]. Cost, efficiency, and durability objectives are shared by fuel cell industrial manufacturers to be competitive in the automotive market.

Fuel cells are complex devices, entailing electrical, thermal, mechanical, and electrochemical interactions at macro- and microscales. Water transport phenomena through the membrane are one of them. PEMFC electrical performance is mainly driven by the perfluorosulfonic acid (PFSA) membrane's ability to conduct protons from cathode to anode. Membrane resistivity is mainly influenced by its hydration state. Water is present in the membrane in a specific phase, and the membrane water content, denoted as λ, is defined as the number of water molecules per sulfonate site. PFSA membranes are deeply investigated in the modern literature [3]. There exists an optimum water content where the membrane has the lowest electrical resistance while maintaining its diffusion capacity. Reaching such an optimum, or diagnosing and avoiding hydration state-related faults, is essential to run PEMFC systems for automotive applications [4] [5].

Water dynamics has been extensively studied in the modeling literature. The temporal variation of the membrane water content is proportional to the net flow gradient through it, in addition to source terms. This has been studied and enhanced with *ex-situ* material characterization. Gass et al. proposed an exhaustive review of these equations [6]. From an experimental point of view, water transport has been studied at a very small cell scale [7]. Nonetheless, there are very few experiments in the literature for bridging the gap between membrane-scale considerations and industrial stack measurements. The main focus of this work is to explain various contributions to water transport at the cell level between the anode and cathode and characterize them experimentally through an innovative water scale method.

II. Cell water balance modeling framework

This section formulates the governing equations for the water flows at the stack inlet and outlet. At the membrane scale, a set of differential equations is set for water content dynamics modeling. Such an approach exists in the literature for different purposes. An experimentally validated cell molar balance model coupled with water content dynamics through the membrane was proposed by Liso et al. [8]. For control applications, a reduced model for water content estimation was developed by Lance et al. [9].

TABLE I
Model parameters and units.

Symbol	Description	Unit
β	Back-diffusion coefficient	-
$\lambda_{a,c}$	Anode, cathode water content	-
λ_m	Membrane water content	-
A_{fc}	Active area	cm^2
c_f	Charge sites concentration	$\mathrm{mol \cdot cm^{-3}}$
D	Effective diffusion coefficient	$\mathrm{cm^2 \cdot s^{-1}}$
F	Faraday constant	$\mathrm{s \cdot A \cdot mol^{-1}}$
j	Current density	$\mathrm{A \cdot cm^{-2}}$
J_{net}	Net water flux	$\mathrm{mol \cdot cm^{-2} \cdot s^{-1}}$
J_{prod}	Produced water flux	$\mathrm{mol \cdot cm^{-2} \cdot s^{-1}}$
J_w	Adsorbed water flux	$\mathrm{molc m^{-2} \cdot s^{-1}}$
n_{cells}	Number of cells	$[-]$
n_d	EOD drag coefficient	-
$\dot{n}_{H_2O,m}$	Net water molar flow	$\mathrm{mol \cdot s^{-1}}$
$\dot{n}_{x,an/ca,in/out}$	Molar flow	$\mathrm{mol \cdot s^{-1}}$
$P_{sat}(T)$	Saturation pressure	bara
$P_{x,an/ca}$	Reactant pressure	bara
$RH_{x,in/out}$	Relative humidity	-
$St_{an,ca}$	Reactant stoichiometry	-

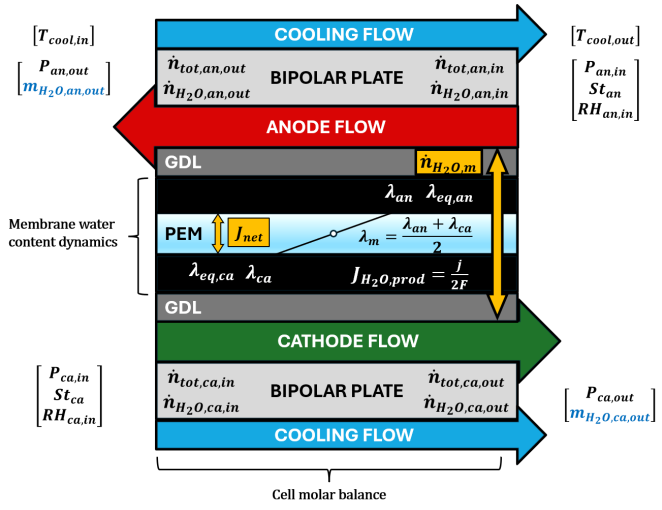


Fig. 1. Modeling framework for PEMFC water transport.

A. Membrane water content dynamics

Membrane water content variation over time is proportional to the gradient of net water molar flux crossing it. This can be modeled by the following partial derivative equation (PDE) reported in many existing models:

$$\frac{\partial \lambda}{\partial t} = \frac{\partial}{\partial x}\left(D(\lambda)\frac{\partial \lambda}{\partial x} + \frac{n_d(\lambda)}{c_f F} j\right) + J_w(\lambda) \tag{1}$$

For convenience, all the model parameters and their corresponding units are listed in Table I. It is known for thin membranes to have a linear through-the-plane water content profile. Therefore, the previous PDE can be simplified in a two-node study at anode and cathode catalyst layer interfaces. This results in a set of two Ordinary Derivative Equations (ODEs):

$$\frac{d\lambda_a}{dt} = \frac{1}{x_{CL}}\left(D(\lambda_{a,c})\nabla\lambda + \frac{1}{c_f}\left(-\frac{n_d(\lambda_{a,c})}{F} j + J_w^a(\lambda_a)\right)\right) \tag{2}$$

$$\frac{d\lambda_c}{dt} = \frac{1}{x_{CL}}\left(-D(\lambda_{a,c})\nabla\lambda + \frac{1}{c_f}\left(\frac{n_d(\lambda_{a,c})}{F} j + J_w^c(\lambda_c)\right)\right) \tag{3}$$

They are completed by an algebraic equation for the membrane water content in the middle of the linear profile:

$$\lambda_m = \frac{\lambda_a + \lambda_c}{2} \tag{4}$$

By focusing on water transport through the membrane, the net flow can be written as the sum of a diffusion and an Electro-Osmotic Drag (EOD) term:

$$J_{net} = c_f D(\lambda_{a,c})\frac{\lambda_c - \lambda_a}{x_m} - \frac{n_d(\lambda_{a,c})}{F} j \tag{5}$$

Thus, the back-diffusion rate is defined as the net molar flux through the membrane, divided by the water production flux of the reaction at the cathode. It is defined in such a referential that a positive flux is directed from the cathode to the anode.

$$\beta = \frac{J_{net}}{J_{prod}} = 2 \cdot \left(\frac{F \cdot c_f}{x_m \cdot j} \cdot D(\lambda_{a,c}) \cdot (\lambda_c - \lambda_a) - n_d(\lambda_{a,c})\right) \tag{6}$$

B. Cell molar balance

Fig. 1 depicts the water transport pathways through the membrane and along the flow channels, in a counter-flow configuration.

1) Cathode inlet: The combined effects of the cathode inlet relative humidity and temperature determine the cathode inlet water flow rate. The total cathode inlet flow rate is a function of the cathode stoichiometric ratio, as expressed below.

$$\dot{n}_{air,ca,in} = A_{fc} \cdot n_{cells} \cdot j \cdot \frac{St_{ca}}{4 \cdot F} \tag{7}$$

$$\dot{n}_{H_2O,ca,in} = \dot{n}_{tot,ca,in} \cdot RH_{ca,in} \frac{P_{sat}(T_{cool,in})}{P_{ca,in}} \tag{8}$$

2) Anode inlet: $X_{H2O,an,in}$ is firstly introduced as the molar fraction at the anode inlet.

$$X_{H_2O,an,in} = RH_{an,in} \cdot \frac{P_{Sat}(T_{cool,out})}{P_{an,in}} \tag{9}$$

$$\dot{n}_{H_2O,an,in} = \frac{X_{H_2O,an,in}}{1 - X_{H_2O,an,in}} \cdot \dot{n}_{H_2,an,in} \tag{10}$$

$$\dot{n}_{H_2,an,in} = A_{fc} \cdot n_{cells} \cdot j \cdot \frac{St_{an}}{2 \cdot F} \tag{11}$$

3) Cell production term: The produced water molar flow rate is proportional to the current drawn and is given by:

$$\dot{n}_{H_2O,prod} = A_{fc} \cdot n_{cells} \cdot \frac{j}{2 \cdot F} \tag{12}$$

4) Net water flow through the membrane: The transfer flow from the cathode to the anode is introduced in the water balance model as $\dot{n}_{H_2O,m}$. Its sign is positive when from the cathode to the anode. As there is no water production at the anode, it is assumed that all the additional water at the anode exhaust side is the result of the transfer flow.

$$\dot{n}_{H_2O,m} = \dot{n}_{H_2O,an,out} - \dot{n}_{H_2O,an,in} \tag{13}$$

The back-diffusion rate β can be consequently written as a metric from the cell molar balance:

$$\beta = \frac{\dot{n}_{H_2O,m}}{\dot{n}_{H_2O,prod}} \tag{14}$$

III. Experimental validation

The goal of this section is to describe the experiments led to characterize water transport in PEMFC industrial stacks.

A. Experimental setup

The experimental setup used for this work is a PEMFC stack characterization testbench from Greenlight. Anodic loop works in flow-through mode, which means there is no hydrogen recirculation. Anode and cathode inlet relative humidities can be controlled separately using a dewpoint temperature regulation mode. It is used in the literature for stack performance assessment [10]. This setup has been completed with scales at anode and cathode drain outlet. Water is condensed, and the condenser is purged once a given liquid volume is reached. Scales are equiped with water collector. The experimental setup together with its corresponding block diagram are represented in Figs. 2 and 3.

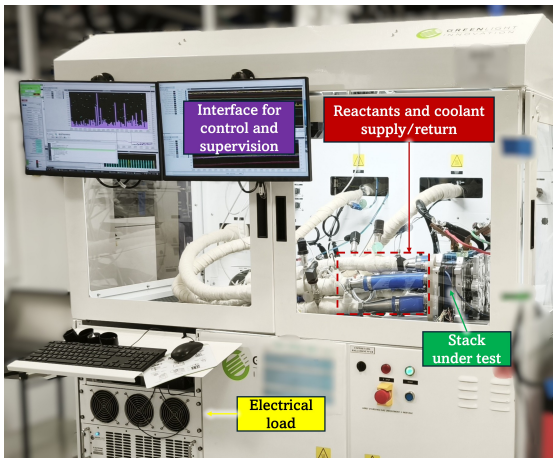


Fig. 2. Experimental test setup.

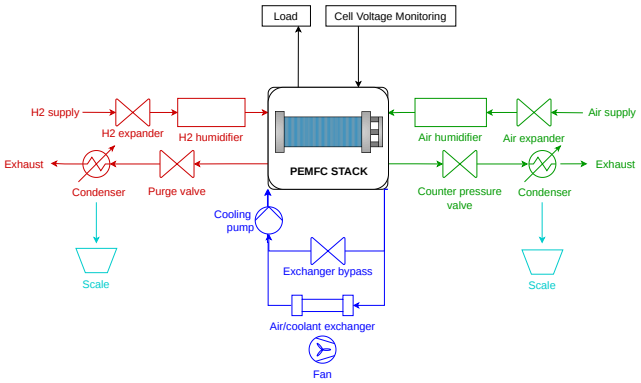


Fig. 3. Block diagram of the PEMFC stack under investigation.

B. Stack used for testing

The stack under test is a NextGen1 stack developed by Symbio. It is part of the commercialized StackPack75 fuel cell system. The 20-cell stack used for testing is however smaller than the 75kW full stack product. Stack break-in has been performed to stabilize BoL (Beginning of Life) performances [11].

C. Experimental test plan

The following test plan has been designed to investigate the sensitivity of water transport to the operating conditions, taking into account the long timespan required for water scaling measurements. Each steady-state operating point requires more than 60 min of testing. The plan has been organized as eleven successive polarization curves. At fixed operating conditions, The overall study focuses on the factors presented in the table below:

TABLE II
Model parameters and units.

Factors	Description/Equation	Unit	Min	Med	Max
∇RH	$RH_{ca,in} - RH_{an,in}$	%	-25	0	35
j		A.cm^{-2}	0.5	1.05	1.6
∇P	$P_{ca,in} - P_{an,in}$	bar	-0.1	0	0.1
$T_{cool,in}$		°C	70	-	77
St_{an}		-	1.8	-	2.5
St_{ca}		-	2.16	-	3

The proposed test plan is fractional. Some points considered as outliers for experimental reasons have been withdrawn from the results. The resulting test matrix is not fully orthogonal. The correlation matrix $\mathbf{R}$ between factors $[\nabla RH, j, \nabla P, T_{cool,in}, St_{an}, St_{ca}]$ entails terms with a 10^{-1} order of magnitude. Interactions between factors are not well-captured in the presented plan. They will be consequently not studied. The obtained test matrix is presented below, with for each operating condition combination its number of repetitions in the test. The operating point taken as reference in the next section is also noted as "REF". Values are coded by levels such as: $\{\text{Min:} -1, \text{Med:}0, \text{Max:}1\}$.

The data collection process is as follows:

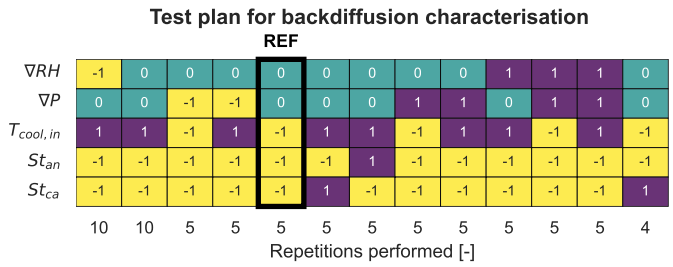


Fig. 4. Experimental test plan matrix.

- The operating conditions are set and stabilisation occurs when every measured condition is within their specified tolerance range.
- Data are averaged over a 60 s time window.
- The operating conditions are maintained until water scale signal reaches a predefined threshold.
- The water collectors placed on the scales are then purged.

Fig. 5 provides a timeline of collected water mass evolution. The steps visible on the plots are due to the water condenser that is purged once a threshold is reached. The accumulated mass noted Δm during a timespan noted Δt for a given steady-state point is depicted on the graph below.

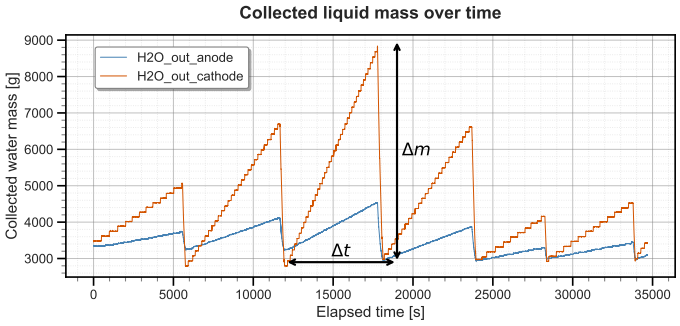


Fig. 5. Water mass collection process.

For data processing, the hypothesis that there is water vapor only in the stack volume is assumed. It means that condensation occurs instantly at test bench outlet, and collected liquid water was exclusively in vapor form inside the stack. Consequently, the liquid water mass evolution is proportional to the vapor flow.

$$\dot{n}_{H_2O,i,out} = \frac{\Delta m_{H_2O,i,out}}{\Delta t \cdot M_{H_2O}}, \quad i \in \{anode, cathode\} \tag{15}$$

The above equations complete the cell molar balance model introduced in the previous section, such that back-diffusion rate can be calculated as:

$$\beta = \frac{1}{\dot{n}_{H_2O,prod}} \cdot \left(\frac{\Delta m_{H_2O,i,out}}{\Delta t \cdot M_{H_2O}} - \dot{n}_{H_2O,an,in} \right) \tag{16}$$

Collected water mass at cathode outlet is included in a conservation equation, to quantify accumulated water during the process. This corresponds to water introduced that is not collected, probably hold inside the test bench. An accumulation rate noted γ is deduced from the conservation equation. In practice, this term is higher than uncertainties calculated on instrumentation. Thus, it is assumed : $\beta_{estimated} = \beta_{measured} \pm \gamma$, with:

$$\gamma = \frac{\Delta m_{H_2O,accumulated}}{\Delta m_{H_2O,prod}} \tag{17}$$

$$\begin{aligned} \Delta m_{H_2O,accumulated} &= \Delta m_{H_2O,introduced,an+ca} \\ &+ \Delta m_{H_2O,prod} - \Delta m_{H_2O,collected,an+ca} \end{aligned} \tag{18}$$

IV. Results and Discussion

A. Back-diffusion sensitivity to operating conditions

In this section, results are presented only for factors $[\nabla RH, \nabla P, T_{cool,in}]$ as coded values introduced in Table II. However, the impact of cathode stoichiometry and current density levels will be studied in the next section. Back-diffusion rate towards selected operating conditions are presented on the bar chart below. Under the operating conditions taken as reference, there is a positive net flow towards anode, despite relatively high accumulation.

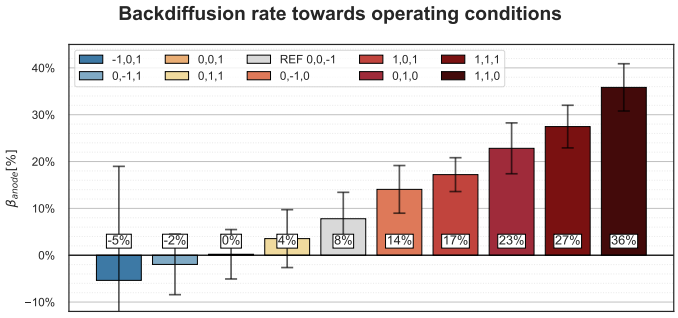


Fig. 6. Back-diffusion rate experimental results.

The back-diffusion is mainly driven by the humidity gradient introduced in reactants. It is even more visible when the gradient is oriented towards th anode. A negative gradient also leads to a cathode-oriented back-diffusion rate, even though its magnitude is way smaller and more impacted by accumulation. Moreover, increasing temperature inhibits the back-diffusion. It is the case by comparing reference conditions with the increase in temperature. It stays however in an area of small diffusion rate with high accumulation. In another extend, the effect of temperature increase is visible for configurations favorable to high back-diffusion rate. By comparing $\{1, 1, 0\}$ and $\{1, 1, 1\}$ for each current step, there is a decrease of 5 to 10% in back-diffusion rate with increasing temperature by only 7°C. This tendency is much more visible by coupling only temperature and cathode overpressure, leading to a 5 to 10 times higher back-diffusion rate. Pressure gradient itself also has an impact on back-diffusion process. Introducing a 100 mbar overpressure on the cathode side can enhance the back-diffusion rate 2 to 3 times compared to the reference. Paradoxically, introducing the same overpressure on the anode side still increases back-diffusion compared to the reference.

It means that diffusion-resulting flow direction does not necessarily go along with the pressure gradient direction. back-diffusion process can be highly triggered by operating conditions. Combining temperature decrease, introduced pressure and humidity gradients, back-diffusion rate can be increased up to 5 times compared to the reference operating conditions.

B. Back-diffusion rate ANOVA study

Based on the collected data, an ANOVA is performed to confirm observations made in the previous section. ANOVA (Analysis Of Variance) is set to evaluate contributions of single factors, and eventually their interaction or quadratic effects on a predicted value. The principle of ANOVA is to split data into groups, and analyze the ratio of between-group variance and within-groups variances. This highlights the fact that differences of variables between groups is not a coincidence. The theory behind it and its application to experimental science has been documented by Sir Ronald Aylmer Fisher [12]. It has been since then widely spread in the literature, with applications to PEMFC performances optimization [13]. The model chosen here is an additive model. It catches only contributions of simple factors, their interactions and quadratic effects are not taken into account. Selected factors for this study are: $[\nabla RH, j, \nabla P, T_{cool,in}, St_{ca}]$. In fact, previously introduced test plan does not entail enough anode stoichiometry variations to include it in the ANOVA. For k factors X_1 to X_k, the model general equation is:

$$Y = \beta_0 + \sum_{i=1}^{k} \beta_i \ X_i + \epsilon \tag{19}$$

where β_0 is a constant and β_i are model coefficients to be fitted. Residuals are noted ϵ, it corresponds to the difference between model prediction and experimental values of the studied variable.

The presented results are obtained using an Ordinary Least Square (OLS) model implemented in Python. It is relevant here as the proposed test plan is not suitable for factor interaction modeling. Results obtained from the model are presented in the table below. After model coefficient fitting, the following

TABLE III
OLS FITTING RESULTS.

Indicator	**Definition**	**Result**
Df Model/Residuals	Degrees of freedom	5/67
R^2	Correlation coefficient	0.922
P(F-stat)	Global model p-value	1.12e-35
Skewness	Residuals distribution symetry	0.006
Kurtosis	Model outliers production	2.275
Durbin Watson	Residuals autocorrelation	1.165

equation can be set for the additive model, using the coded values:

$$\beta = 1.9559 + 15.5884 \cdot \nabla RH - 1.7519 \cdot j + 4.4685 \nabla P - 6.2100 \cdot T_{cool,in} - 6.6052 \cdot St_{ca} \tag{20}$$

Once the proposed model is considered appropriate for the study, a type 2 ANOVA is performed. As the order of factors in the model does not have any importance, a type 1 is not suitable. The influence of each factor should be evaluated separately, which is not possible with a type 3 ANOVA. Once the model coefficients are fitted and the ANOVA performed, the relative square sum of each factor is presented on the pie chart, as shown in Fig. 7.

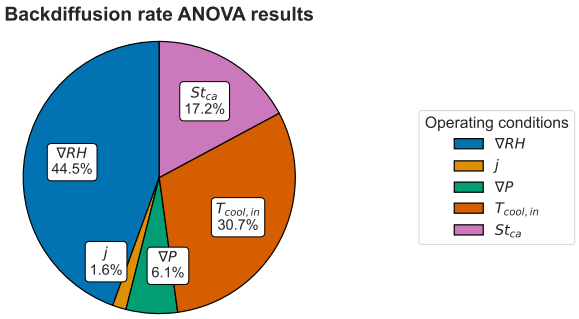


Fig. 7. Back-diffusion rate contributors.

Firstly, ∇RH is identified as the main contributor to the back-diffusion rate variations, with more than 44% of the explained total square sum, confirming previous observations. Besides, $T_{cool,in}$ represents more than 30% of the back-diffusion rate variations Current density j has a very small effect on back-diffusion rate. There is a difference between mechanistic and experimental modeling of back-diffusion rate dependency on current density. The pressure gradient ∇P has a relatively small impact on back-diffusion, with only 6% of total square sum explained. This term does not appear in the membrane net flow model, but its impact is not negligible at the stack level. This can be explained by the fact that pressure gradient is linked with multiple phenomena at the membrane scales. Among them is the increase in water vapor pressure, which directly impacts relative humidity gradient. Membrane permeation can also be triggered by gas pressure. Finally, cathode stoichiometry ratio St_{ca} is significant in the proposed additive model. The sign of its associated coefficient in the previous equation is negative, which means that increasing the cathode flow rate reduces diffusion towards the anode side. The physical explanation behind is the capacity of the cathode flow rate to expel produced water directly at the cathode outlet.

C. Model application

In this section, the obtained additive model is compared with physical steady-state equation resulting from the modeling of membrane water transport dynamics. Equation (6) is displayed in the figure below, using parameters provided in [9].

The black line corresponds to a no-back-diffusion regime where the water contents at the anode and cathode sides are equal. The grey area between this line and the contour map is mainly due to the Electro-Osmotic Drag (EOD) phenomena, which depends on the current drawn. The contour map itself presents back-diffusion rate iso-lines, depending

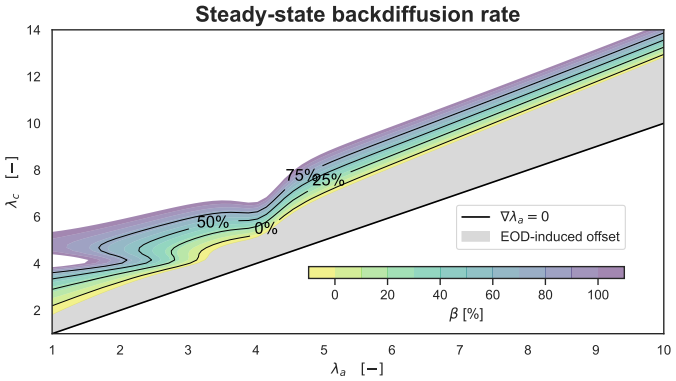


Fig. 8. Steady-state back-diffusion rate.

on the membrane water content values at the anode and cathode sides. Equation (6) is sensitive to current density and temperature. These parameters are also modeled in the multilinear model (20). However, other operating conditions such as $\nabla RH, St_{ca}, \nabla P$ are only accounted in the multilinear model. Consequently, the two presented models can be used to estimate the possible values for the membrane water content. For a given set of operating conditions, the back-diffusion rate can be predicted using (20), and the iso-lines provided in Fig. 8 depicts possible combinations for $\{\lambda_a, \lambda_c\}$. Coupling the two models would require a more accurate modeling framework through the membrane, as presented in Fig. 1.

V. Conclusions and perspectives

The presented work provides an overview of back-diffusion rate characterization and sensitivity in multiple steps:

- A test plan has been proposed to quantify operating condition contributions using water scales at anode and cathode outlets. This test plan does not catch interactions between factors and quadratic effects. A reduced quasi-ortogonal test plan such as a Box-Behnken one should be performed, to catch interactions between parameters.
- An ANOVA has been performed to assess the respective contributions of the operating factors, and their respective coefficients within a additive model have been fitted using multilinear regression. As a result, ANOVA confirms tendencies observed on experimental processed data. More than 90% of the experimental data are predicted by the model. Relative humidity gradient and coolant temperature explain more than 75% of the total variance, confirming the Fickian-like diffusion behaviour and its temperature dependancy. The proposed model is however limited and could be improved. A polynomial model could predict the back-diffusion rate through Response Surface Method (RSM) with a higher accuracy, for instance towards gas pressure and relative humidity coupling.
- The experimental model has been complemented by an algebraic equation derived from the steady-state form fo the ODEs modeling water content dynamics inside the membrane. In this way, the proposed approach bridges controllable test bench operating conditions with microscale membrane water transport modeling. A model coupling between the two equations should improve the global model prediction capacity.

This work paves the way for experimental model integration in model-based control algorithms. Such models can provide valuable insights for observer measurement equations, and enable PEMFC internal state observation using a limited number of sensors.

Acknowledgment

This work has been supported by the European Union (Next Generation EU), the French State (France 2030, France Relance), the EIPHI Graduate School (contract ANR-17-EURE0002) and the Region Bourgogne Franche-Comté.

References

[1] Hussein Togun et al., 'Development and comparative analysis between battery electric vehicles (BEV) and fuel cell electric vehicles (FCEV)', Applied Energy, vol. 388, p. 125726, Jun. 2025, doi: 10.1016/j.apenergy.2025.125726.

[2] Zikuo Liu et al., 'Recent development in degradation mechanisms of proton exchange membrane fuel cells for vehicle applications: problems, progress, and perspectives', Energy Storage and Saving, vol. 3, no. 2, pp. 106–152, Jun. 2024, doi: 10.1016/j.enss.2024.02.005.

[3] Ahmet Kusoglu et al., 'New Insights into Perfluorinated Sulfonic-Acid Ionomers', Chem. Rev., vol. 117, no. 3, pp. 987–1104, Feb. 2017, doi: 10.1021/acs.chemrev.6b00159.

[4] J. Aubry et al., 'Fuel cell diagnosis methods for embedded automotive applications', Energy Reports, vol. 8, pp. 6687–6706, Nov. 2022, doi: 10.1016/j.egyr.2022.05.036.

[5] Zhiguang Hua et al., 'Multi-Timescale Lifespan Prediction for PEMFC Systems Under Dynamic Operating Conditions', IEEE Trans. Transp. Electrific., vol. 8, no. 1, pp. 345–355, Mar. 2022, doi: 10.1109/TTE.2021.3103921.

[6] Raphaël Gass et al., 'A Critical Review of Proton Exchange Membrane Fuel Cells Matter Transports and Voltage Polarisation for Modelling', Journal of The Electrochemical Society, vol. 171, no. 3, p. 034511, Mar. 2024, doi: 10.1149/1945-7111/ad305a.

[7] Tim Dörenkamp et al., 'Investigation of Dynamic Water Cluster and Droplet Interactions in Polymer Electrolyte Fuel Cells using Operando X-ray Tomographic Microscopy', J. Electrochem. Soc., vol. 171, no. 9, p. 094505, Sep. 2024, doi: 10.1149/1945-7111/ad749f.

[8] Vincenzo Liso et al., 'Modeling and experimental validation of water mass balance in a PEM fuel cell stack', International Journal of Hydrogen Energy, vol. 41, no. 4, pp. 3079–3092, Jan. 2016, doi: 10.1016/j.ijhydene.2015.10.095.

[9] Gontran Lance, 'Adaptive extended kalman filter for PEMFC membrane water content estimation', International Journal of Hydrogen Energy, 2024.

[10] Martin Serine et al., 'Development of a humidity estimation tool for automotive PEMFC stacks'.

[11] F. Van Der Linden et al., 'A review on the Proton-Exchange Membrane Fuel Cell break-in physical principles, activation procedures, and characterization methods', Journal of Power Sources, vol. 575, p. 233168, Aug. 2023, doi: 10.1016/j.jpowsour.2023.233168.

[12] 'The design of experiments - Google Books'. [Online].

[13] Prem Kumar Thiyagarajan et al., 'Investigating the combinations of operating parameters of PEMFC computational results using the Taguchi Method', International Journal of Thermofluids, vol. 27, p. 101162, May 2025, doi: 10.1016/j.ijft.2025.101162.

[14] Bouchra Wahdame et al., 'Analysis of a PEMFC durability test under low humidity conditions and stack behaviour modelling using experimental design techniques', Journal of Power Sources, vol. 182, no. 2, pp. 429–440, Aug. 2008, doi: 10.1016/j.jpowsour.2007.12.122.